ARCHIVES
of
FOUNDRY ENGINEERING
10.24425/afe.2026.157987
Published quarterly as the organ of the Foundry Commission of the Polish Academy of Sciences
ISSN (2299-2944)
Volume 2026
Issue 2/2026
33 – 41
4/2

Optimizing Resin Dosage and Sand Grading to Enhance the Properties of 3D-Printed Furan Sand Molds

Han Zheng [a], Xinhan Zhu [a], Guoqiang Zhang [b], Fengguo Liu [a], Xianfei Zhang [a], Changsheng Lou [a, *]
[a] School of Materials Science and Engineering, Shenyang Ligong University, Shenyang 110159, Liaoning, China.
[b] Liaoning Lianxin Foundry Sand Investment Group Co., Ltd., Shenyang 110000, Liaoning, China
* Corresponding author: E-mail address: chsh_lou@163.com

Received 23.12.2025; accepted in revised form 04.02.2026; available online 24.06.2026

Abstract

This study investigates the influence of resin content, curing agent ratio, curing time, and sand grading on the strength, gas permeability, and gas evolution behaviours of furan resin sand molds in 3D printing-based sand casting. The focus is on optimizing material usage and aligning with sustainable manufacturing objectives to minimize the waste. A multivariate quadratic polynomial regression model was developed through orthogonal experiments and microstructural characterization. The findings indicate that the addition of furan resin is crucial for determining the tensile strength, gas evolution, and permeability of sand molds. Under the process parameters of 2.0% resin content, 40% curing agent ratio, and 24-hour curing time, the sand mold demonstrated a tensile strength of 2.98 MPa, gas evolution of 10.4 mL/g, and permeability of 119.3 AFS. Further increasing the resin content beyond 2.0% resulted in a plateau in the strength gain, accompanied by a sharp increase in gas evolution. The application of an optimized sand grading ratio of 3 parts coarse (150-212 μm) to 7 parts fine (106-150 μm) led to comprehensive performance improvements: the tensile strength increased to 3.02 MPa, gas evolution was controlled at 11.2 mL/g, packing density approached theoretical optimum values, and surface roughness was significantly reduced to a Sa value of 43.478 μm. This study formulates a multi-objective optimization framework and strengthens the theoretical basis for furan resin sand molding in 3D printing, providing industrially viable solutions to minimize typical defects, such as gas porosity and sand adhesion, in real-world casting operations.

Keywords: 3D printed sand molds, Furan resin content, Sand grading, Tensile strength, Permeability

1. Introduction

Achieving sustainable development in the foundry industry requires addressing challenges from high pollution and resource consumption in resin sand processes. The global foundry sector uses tens of millions of tons of molding sand annually. Excessive resin binders cause resource wastage and environmental pollution through volatile organic compound emissions during production and gas evolution during casting. Research shows that a marginal 1% reduction in resin usage results in a disproportionate 5–8% decrease in emissions and resource consumption, underscoring its critical role in the green transition [1-3]. In rapid sand mold manufacturing, 3D printing (3DP) has emerged as a leading solution due to material adaptability, mold-free nature, and cost-effectiveness [4-7]. The technology involves jetting liquid binders, such as furan, phenolic, or silicate-based inorganic binders, for layer-by-layer sand curing [8-12].

However, challenges include low sand core strength, high resin consumption, and excessive gas evolution. The ratio of binder to curing agent critically influences sand mold performance [13-16]. In traditional resin sand processes, furan resin typically constitutes

1.5%–2.5% of raw sand mass, where resin-sand strength performance is optimal. This value requires adjustment based on sand particle size, curing agent ratio, and ambient temperature. In 3DP sand mold processes, furan resin addition is higher, accounting for 2.13–3.6% of silica sand mass. Higher resin content meets bonding strength and molding accuracy requirements during printing but requires gas evolution control. For current 3DP-printed sand cores, increased resin addition improves bonding strength and molding accuracy, but gas evolution increases [17-19]. This reflects a cycle of high-strength demands, high resin usage, and high pollution emissions. While studies have improved sand mold mechanical properties through particle size distribution optimization [20], data on optimal resin addition ranges remain insufficient. Increasing resin content to meet strength requirements leads to higher gas evolution, compromising casting quality and environmental impact [21-22].

This study examined the evolution of sand mold performance under reduced resin consumption by integrating multi-level sand grading optimization with modifications in furan resin-curing agent ratio. The focus is on analyzing how grading optimization can reduce resin usage while enhancing mold properties and mitigating defects. The study examined changes in sand mold performance from modifications in the resin-curing agent system. Variations in mold strength, gas evolution, and permeability were assessed by reducing resin dosage. The synergistic effects of sand grading and resin ratio adjustments on improving mold performance were explored. This approach ensures quality while reducing emissions and resource consumption, providing technical support and theoretical basis for promoting 3DP-printed sand molds in efficient, low-cost, high-quality casting processes [23].

2. Experimental processes

2.1. Experimental Materials

The raw material used in this experiment was AS-15-3 3D printing silica sand supplied by Zhangwu Lianxin Casting Sand Group. The SEM images and particle size distribution of the 3D silica sand are shown in Figure 1. This sand exhibits extremely low clay content at 0.05 %, minimal moisture content at 0.03 %, and a low loss on ignition at 0.06 %. Its high purity contributes to improved resin bonding efficiency, enhanced sand mold strength, and significantly reduced gas evolution during pouring. Additionally, its low acid demand value at 0.6 ml enables reduced resin addition, further controlling gas generation. In terms of physical properties, the sand features a favorable angularity coefficient and excellent fluidity at 56 s, which promotes uniform sand spreading and molding accuracy. Its moderate bulk density at 1.56 g/mL aids in forming dense sand mold surfaces, thereby improving overall sand mold quality.

The specialized 3D printing furan resin model SZ3DPRF and matching water-based curing agent model SZ3DHS, form a high-performance material system specifically designed for binder jetting technology. This resin-curing agent system collectively guarantees excellent molding accuracy, high strength, and low gas evolution characteristics for 3D printed sand molds, making it suitable for producing complex, precision castings.

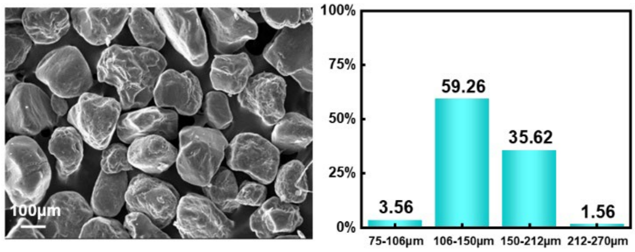

Fig. 1. Microstructure and particle size distribution of 3D printed silica sand

2.2. Specimens Preparation

The standard sand specimens were prepared as shown in Figure 2. The 3D printing silica sand was precisely weighed and subsequently subjected to a drying process in an infrared dryer for a duration of 20 minutes. Following the drying procedure, the sand was allowed to cool naturally for one hour. The 3D printing sand, curing agent, and furan resin were then sequentially introduced into a sand mixer for mixing, with each cycle lasting approximately 60 s. The samples were fabricated using a resin-sand sample maker Six parallel samples were prepared for each group. Initially, sampling was conducted, and the resulting samples were placed in a designated area for storage. The prepared samples comprised dog-bone-shaped tensile, bending, and permeability sand specimens.[24].

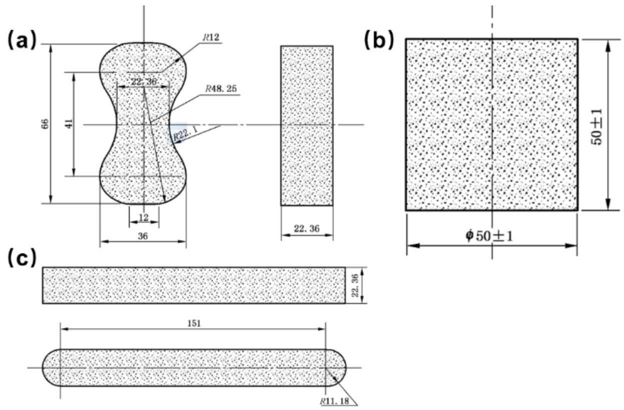

Fig. 2. Schematic diagram of standard sand specimen. (a) shows the tensile strength specimen of the sand mol; (b) the permeability specimen; and (c) the bending strength specimen

The mixing ratios of the resin sand are listed in Table 1, totalling 18 groups. The resin-to-sand ratio ranged from 0.8% to 2.8% (Building upon the conventional process range of 1.5%-2.5% and the 3D printing process range of 2.13%-3.6%, the scope was expanded to 0.8%-2.8% to encompass the full performance interval) [13–16], and the curing agent-to-resin ratio was set at 30%, 40%, and 50% (Based on the technical specifications of the resin and curing agent, the supplier-recommended range is 30%–50%, with reference to conventional industry ratios). The results for each group were measured at curing times of 4, 24, and 48 h (4h represents the early-stage strength, 24h is the standard curing time, and 48h is used for long-term stability testing).

A multi-factor orthogonal rotary combination design was implemented based on the peripheral range values of the single-factor optimization results. The coding of the factor levels is presented in Table 2. Regression models for the tensile strength, bending strength, and gas evolution of the sand molds were developed.

Table 1.
Resin Formulation Experimental Design

Experimental group	The ratio of curing agent content to resin/%	The resin content relative to the sand/%	Experimental group	The ratio of curing agent content to resin/%	The resin content relative to the sand/%
T1	30	0.8	T10	40	2.0
T2	30	1.2	T11	40	2.4
T3	30	1.6	T12	40	2.8
T4	30	2.0	T13	50	0.8
T5	30	2.4	T14	50	1.2
T6	30	2.8	T15	50	1.6
T7	40	0.8	T16	50	2.0
T8	40	1.2	T17	50	2.4
T9	40	1.6	T18	50	2.8

Table 2.
Factors and Levels of Orthogonal Experiment

Level	A: Resin Addition (%)	B: Curing Agent Addition (%)	C: Curing Time (h)
-1	0.8	30	4
0	2	40	24
1	2.8	50	48

As the aforementioned experiments mentioned in Ref. [25], when the ratio of the small to large sphere radii is 0.643, the maximum theoretical density of 0.746 g/cm³ can be achieved in an ordered orthorhombic lattice packing. Although disordered packing may approach this value through an optimized size distribution, the ordered structure remains the theoretically optimal solution. According to reference [26], the density increases when the ratio is less than 0.70. Therefore, sands with size ranges of 106-150μm (100-140 mesh) and 150-212μm (70-100 mesh) were selected for mixing. The average particle size ratio of these two sand ranges was 0.707, which is close to the aforementioned value. Table 3 is based on a single-factor variable design, with the mixing ratio of coarse sand to fine sand as the sole variable.

Table 3.
Sand Grading Experimental Design

Group	150-212μm Sand Proportion (%)	106-150μm Sand Proportion (%)	Group	150-212μm Sand Proportion (%)	106-150μm Sand Proportion (%)
S1	100	0	S7	40	60
S2	90	10	S8	30	70
S3	80	20	S9	20	80
S4	70	30	S10	10	90
S5	60	40	S11	0	100
S6	50	50			

2.3. Sand Mold Testing

Computed tomography (CT), scanning electron microscopy (SEM), and laser confocal microscopy were used in combination to analyze the sand-mold structure [27-30]. CT tests adopted the ZEISS Versa 620 with parameters: 100 kV voltage, 140 μA current, and 0.5 μm voxel. It visualized the internal microstructure of sand particles, revealed particle grading's influence on spatial structure, and enabled quantitative analysis of pore distribution, packing state, and connectivity, providing a 3D perspective for exploring gas permeability and particle mechanical interlocking correlations.

The JEOL JSM-6360LV was used with key parameters: 3.00 kV accelerating voltage, 10.0 mm working distance, ×100 magnification, Std.P.C. detector mode, 1280×960 μm FOV, and LDF mode. It analyzed sand particle surface morphology, resin distribution, and bonding bridge microcharacteristics, measuring thickness and contact area, while verifying grading design rationality and microscopic mechanisms of tensile strength and permeability.

Characterization employed the PONY X200 with Creation + Recommended HD scanning mode, Detail measurement mode, Gaussian Filter, and Height/Mix analysis mode. Key parameters included V-parameter (p=10%, q=80%) and Sxp-parameter (p=2.5%, q=50%) area ratios, and c=0.2 correlation threshold. It obtained sand mold surface 3D topology and quantified roughness indices like Sa and Sq, directly evaluating casting surface defect risks.

3. Results and Discussion

3.1. Effect of Resin Formulation on Sand Mold Properties

The effects of resin formulation on tensile strength of sand molds when curing agent at various conditions were presented in Figure 3. It's well known that the ratio of furan resin to curing agent is a critical parameter in process control, as variations in their proportions decisively influence the sand molds performance. In this experiment, under constrained conditions where the curing agent dosage was maintained at 30%, 40%, and 50% of the resin mass, the effect of different resin addition levels on the tensile strength of sand molds at curing times of 4, 24, and 48 h was investigated. The test data obtained from this experiment yielded the following results: The influence of varying resin addition amounts on the gas evolution and permeability of sand molds after 24 h of curing was also studied.

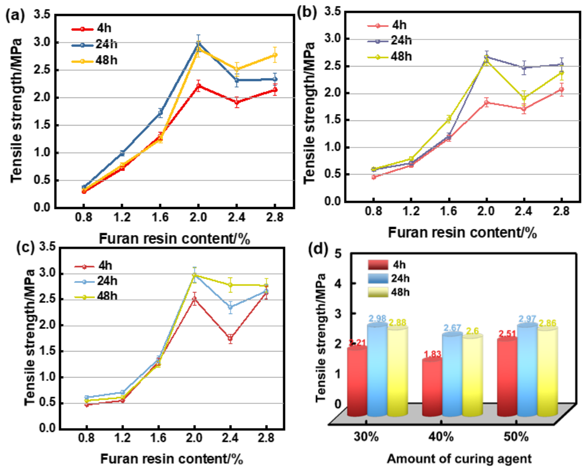

Fig. 3. Effects of resin content and curing agent content on the tensile strength at different curing times (in hours). (a) Relationship between tensile strength and resin content at a curing agent content of 30%; (b) at a curing agent content of 40%; (c) at a curing agent content of 50%; (d) Comparison of tensile strength of sand molds at 2% resin addition (relative to sand mass)

The experimental results indicated in Figure 3 and Figure 4 shows that, when the curing agent ratios are 30%, 40%, and 50%, the tensile strength of the sand molds ranges from 0.29–2.98 MPa, 0.45–2.67 MPa, and 0.47–2.98 MPa. The maximum strength of 2.98 MPa was achieved at 2.0% resin addition, 24 h curing time, and 30% or 50% curing agent ratio. The maximum strength at a 40% curing agent ratio was 2.67 MPa. Gas evolution varied with resin addition: at curing agent ratios of 30%, 40%, and 50%, the values were 6–12.5, 6.3–13.1, and 7.1–13.3 ml/g, respectively. At 2.0% resin addition, the gas evolution was 10.4 ml/g. With a fixed curing time of 24 h, the permeability ranged between 108 AFS and 158.9 AFS. The highest permeability of 158.9 AFS was observed at 0.8% resin addition and 40% curing agent ratio, while the lowest value of 108 occurred at 2.4% resin addition and 50% curing agent ratio. At 2.0%, a resin addition of 40% curing agent ratio, the permeability was 119.3 AFS.

Notably, the strength after 48 h of curing is slightly lower than that after 24 h. This is mainly due to the over-curing phenomenon of furan resin: the cross-linking reaction of resin is basically completed at 24 h, forming a dense three-dimensional network structure; at 48 h, prolonged curing leads to the fracture of some cross-linking bonds, increasing the brittleness of the resin film and thus slightly reducing the strength of the sand mold.

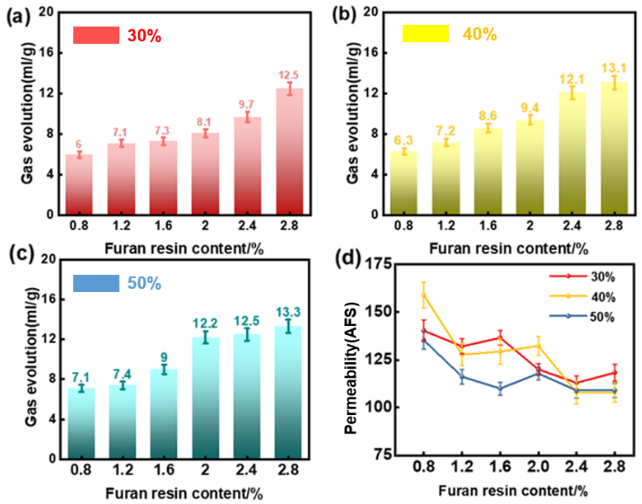

Fig. 4. Effects of resin addition and curing agent addition on gas evolution and permeability of sand molds at 24-hour curing time. (a) Relationship between gas evolution rate and resin content at a curing agent ratio of 30%;(b) At a curing agent ratio of 40%;(c) At a curing agent ratio of 50%;(d) Relationship between gas permeability and curing agent ratio under 24-hour curing condition

3.2. Analysis of Orthogonal Multi-Factor Simulation Results

The analysis of the multifactor simulation results was conducted based on an orthogonal rotary design. Using the values of each influencing factor as independent variables and the tensile strength, gas evolution, and permeability of the sand molds as evaluation indicators, the simulation results are shown in Table 4.

Table 4.
Orthogonal Experimental Design

Group	A	B	C	Tensile Strength (MPa)	Gas Evolution (mL/g)	Permeability (AFS)
1	0.8	30	24	0.37	6	140.3
2	2.8	30	24	2.33	12.5	118.3
3	0.8	50	24	0.61	7.1	135.3
4	2.8	50	24	2.66	13.3	109
5	0.8	40	4	0.45	6.3	158.9
6	2.8	40	4	2.07	13.1	108
7	0.8	40	48	0.6	6.1	150
8	2.8	40	48	2.38	12.9	110
9	2	30	4	2.21	8.2	122
10	2	50	4	2.51	12.4	117.9
11	2	30	48	2.88	8.3	120
12	2	50	48	2.97	12.1	119
13	2	40	24	2.67	10.1	132.3
14	2	40	24	2.56	10.4	135.6
15	2	40	24	2.58	11	130.1
16	2	40	24	2.88	10.7	129.6
17	2	40	24	2.87	11.2	131.1

Based on the experimental data, quadratic polynomial regression models for the tensile strength, gas evolution, and permeability of the sand molds were established as follow.

$$Y_1=2.59+0.93A+0.12B+0.19C+0.02AB+0.05AC-0.05BC-1.10A^2+0.024B^2-0.113C^2 \quad (1)$$

$$Y_2=10.02+3.29A+1.23B-0.08C+0.08AB+0.02AC-0.04BC-0.015A^2-0.15B^2-0.27C^2 \quad (2)$$

$$Y_3=135.18-17.29A-2.30B-1.21C-0.84AB+2.33AC+0.88BC-0.51A^2-9.03B^2-2.94C^2 \quad (3)$$

where Y_1 is the tensile strength of the sand mold, Y_2 is the gas emission rate, Y_3 is the permeability of the sand mold, A is the amount of resin added, B is the amount of curing agent added, and C is the curing time.

High p-value terms are retained to maintain the integrity of the multivariate quadratic polynomial regression models and to account for potential factor interactions. The overall models remain highly significant ($p<0.0001$) with R^2 values close to 1, ensuring reliable predictions.

Based on experimental design and regression modelling, the optimal parameters for the furan sand mold are determined via multi-objective optimization, balancing tensile strength, gas evolution, and permeability.

Based on the variance analysis results of the regression models shown in Table 5, it can be concluded that the P-values for all regression models are below 0.0001, indicating that the models are highly statistically significant. The P-values for the lack-of-fit terms were all greater than 0.05, suggesting that the lack of fit was not significant and that the models exhibited a high degree of correlation. Analysis of the P-values for the resin addition, curing agent addition, and curing time revealed that these three experimental factors had extremely significant effects on the tensile strength, gas evolution, and permeability of the sand molds. The factors influencing the tensile strength of the sand molds, in descending order of impact, are resin addition, curing time, and curing agent addition.

For gas evolution, the order of influence was resin addition, curing agent addition, and curing time. Regarding permeability, the influencing factors were resin addition, curing agent addition, and curing time. In the regression models for tensile strength, gas evolution, and permeability, the p-values for all interaction terms were less than 0.05, indicating that the interactions among the three terms were statistically significant. The coefficients of determination (R^2) and adjusted coefficients of determination for all three models were close to 1. The coefficients of variation and signal-to-noise ratios were 8.05%, 9.69%, 5.78% and 20.19, 12.08, 8.45, respectively, demonstrating that the established regression models possessed high predictive accuracy and reliability.

Table 5.
Analysis of Variance for Quadratic Polynomial Model of Sand Mold Performance

Source	Tensile Strength		Gas Evolution		Permeability	
	Sum of Squares	p-value	Sum of Squares	p-value	Sum of Squares	p-value
Model	13.95	<0.0001	101.58	<0.0001	2855.7	0.0145
A	6.87	<0.0001	86.15	<0.0001	2383.01	0.0003
B	0.11	0.0964	11.79	0.0097	41.38	0.4096
C	0.30	0.0146	0.0459	0.8324	11.36	0.6584
AB	0.013	0.8341	0.0237	0.8790	2.85	0.8244
AC	0.01	0.5773	0.0009	0.8790	22.33	0.5400
BC	0.012	0.5376	0.0039	0.9762	3.13	0.8162
A2	4.62	<0.0001	0.0372	0.9506	0.7017	0.9123
B2	0.0023	0.7825	0.0443	0.8488	278.19	0.0571
C2	0.052	0.2173	0.2042	0.8352	17.09	0.5906
Residual	0.20		6.66		376.6	
Lack of Fit	0.10	0.3557	4.79	0.1329	250.39	0.1853
Pure Error	0.096		1.87		126.21	
Cor Total	14.14		108.24		3232.3	

3.3. Effect of Sand Grading on Sand Mold Properties

The tensile strength of resin–sand molds is influenced not only by sand grading but also by the amount of resin added, curing agent type, and dosage. These factors interact complexly with sand grading to collectively determine the final performance of sand molds. As 3D printing silica sand serves as the sole aggregate for furan resin sand, optimizing its particle size distribution can achieve a denser skeleton structure while reducing the sand porosity and total surface area. This subsequently decreases the binder consumption and lowers the production costs [31]. When the resin addition was 2% and the curing agent dosage was 40% of the resin mass, variations in the proportion of 150-212μm sand to 106-150 μm sand led to changes in the tensile and bending strengths of the sand molds, as shown in Figure 5 (a) and (b). Similarly, under the same conditions (2% resin addition and 40% curing agent relative to resin), changes in the proportion of 150-212μm sand to 106-150μm sand resulted in variations in the gas evolution and permeability of the sand molds, as illustrated in Figure 5 (c) and (d).

As shown in Figure 5, as the proportion of 150-212μm coarse sand decreased from 100% to 30%, the tensile strength initially increased and then decreased, reaching a peak value of 3.02 MPa at a ratio of 3:7 (coarse-to-fine sand). This trend is attributed to changes in the sand particle packing state: excessive coarse sand results in a loose skeleton and elongated resin bridges, leading to insufficient strength, and increasing fine sand effectively fills pores, reducing porosity. Optimized grading simultaneously influences gas evolution behavior and permeability.

Meanwhile, as the coarse-to-fine sand ratio changed from 10:0 to 0:10, the gas evolution first decreased and then increased. A high coarse sand content yields high porosity and low resin usage, providing good permeability but low strength. When the fine sand proportion increased to 3:7, the packing became dense with uniform resin coating, stabilizing the gas evolution at 11.2 mL/g. Permeability decreases due to reduced pore connectivity [32-34]. This phenomenon reflects the effect of grading on the packing. At the 3:7 ratio, fine sand fills the gaps between coarse sand particles, consistent with the literature [25] stating that "particle grading regulates resin distribution via specific surface area." Moreover, the particle size ratio of 0.714 at this point was close to the theoretical optimum of 0.643 [26], achieving the maximum packing density. This ensures strength while reducing the risk of gas-pore formation.

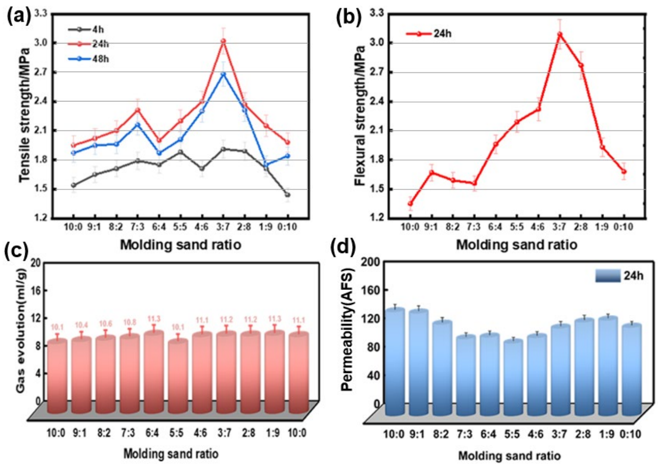

Fig. 5. Effects of Sand Formulation Ratio on Material Tensile Strength, Bending Strength, Gas Evolution, and Permeability. (On the horizontal axis, a ratio of 10:0 represents 100% coarse sand with a particle size of 150–212 μm, while a ratio of 0:10 represents 100% fine sand with a particle size of 106–150 μm)

3.4. Morphology, Microstructure, and Surface Roughness

To investigate the effects of single-particle size distribution and particle size grading on the mechanical properties of sand mold specimens, it is essential to observe and analyze the microstructure of the fracture surfaces at the microscale. The overall microstructure was studied using scanning electron microscopy (SEM). Subsequently, the bonding necks of the specimens were further examined, as shown in Figure 6, where the bonding necks are indicated by the red circles.

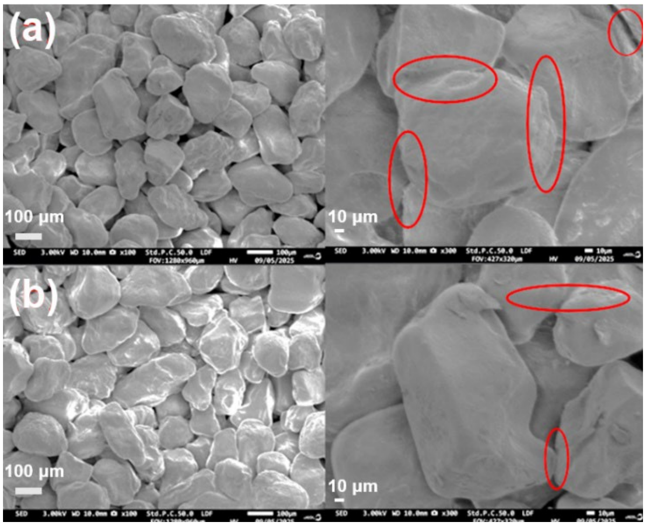

Fig. 6. (a) and (b) show the SEM images of the 3:7 graded sand mold and raw sand mold, respectively, with bonding necks indicated by red circles

To further characterize the internal particle packing and pore structure of the sand mold, Computed Tomography (CT) was used to visualize the microstructure of the sand particles. Figure 7 shows the CT scan images of the silica sand particles in the 3D printed sand mold, presenting their morphological characteristics and spatial distribution. The clear boundaries and pore spaces observed in the CT scans provide direct evidence of the effect of particle grading on gas permeability and mechanical interlocking.

The surface roughness of sand molds is a critical factor that influences casting quality, directly affecting the surface finish of castings, demolding difficulty, and subsequent cleaning costs. In this study, sand sample A (prepared by mixing 150-212μm sand and 106-150μm sand) and sand sample B (fabricated using 3DP silica sand) were compared to analyze the differences in their surface morphologies. A confocal laser scanning microscope (CLSM) was used to perform non-contact three-dimensional scanning of the sample surfaces. By acquiring high-resolution 2D images and 3D topography data, three-dimensional roughness parameters, including the arithmetic mean deviation (Sa) and root mean square deviation (Sq), were extracted.

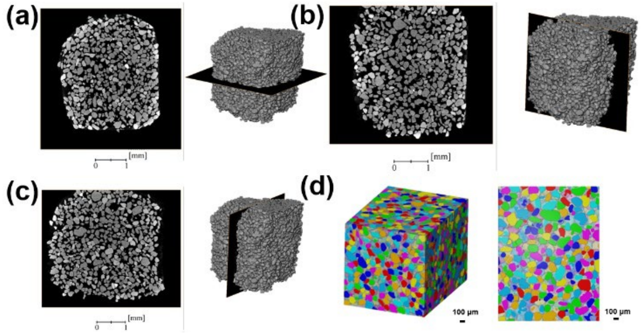

Fig. 7. CT scan images of silica sand particles used in 3D printed furan resin sand mold. (a), (b), and (c) refer to section images of different orientations and surfaces from the same sand mold specimen

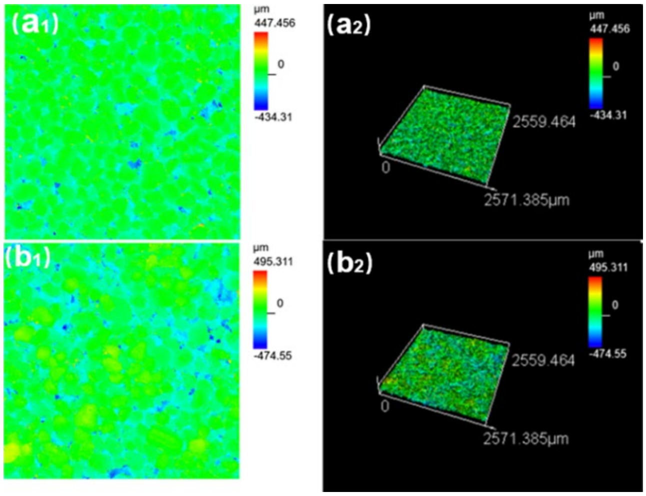

Fig. 8. 2D and 3D CLSM images of the sand molds

Quantitative analysis based on the 3D topographic data obtained by CLSM revealed significant differences in the surface roughness between the two sand samples. As shown in Figure 8, the 3D topography of sample A (a_2) exhibited relatively gentle undulations, with a calculated three-dimensional arithmetic mean height (Sa) of 43.478μm and a root mean square height (Sq) of 59.106μm. In contrast, sample B demonstrated sharper peak-valley structures and a more complex texture distribution, with both Sa (66.3μm) and Sq (85.581μm) values significantly higher than those of sample A. These findings were visually confirmed in the 2D grayscale images (Figure 6 a_1, b_1): the image of sample B shows higher contrast in light-dark variations, indicating greater height fluctuations and rougher surface topography. The smoother surface of sample A is expected to yield a superior casting surface quality and lower friction resistance during the casting process, whereas the rougher surface of sample B may require additional coating coverage or face higher risks of sand adhesion to castings.

4. Conclusions

In this study, the influence of resin content, curing agent ratio, curing time, and sand grading on the performance of furan resin sand molds for 3D printing was investigated. These findings highlight the significant impact of resin content on the tensile strength, gas emission, and permeability of sand molds, offering an effective approach for optimizing the 3D printing sand mold process. These results contribute to enhancing the strength and efficiency of 3D printed sand molds while addressing the challenges of high resin consumption and gas emissions.

1) This study demonstrated that the resin content significantly influences the mechanical properties of sand molds, including tensile strength, gas emission, and permeability. When the resin content was optimized to 2.0% with a curing agent ratio of 40% and curing time of 24 h, the sand mold exhibited the highest tensile strength of 2.98 MPa, with controlled gas emissions and permeability. This confirms the critical role of resin content in balancing the mold strength and minimizing defects such as gas porosity.
2) This study also revealed the effectiveness of optimizing sand grading in conjunction with resin content. By adjusting the coarse-to-fine sand ratio to 3:7, the study found a significant improvement in tensile strength to 3.02 MPa, while reducing surface roughness and gas emissions, which are essential for improving molds quality and reducing casting defects.

Acknowledgements

The authors would also like to acknowledge support from the Liaoning Province Central Guidance for Local Science and Technology Development Special Project (2024JH6/100300008).

References

[1] Oguntuyi, S.D., Nyembwe, K., Shongwe, M.B., Kabasele, J., & Mojisola, T. (2025). A review of the influence of sand properties on parts manufactured by rapid sand casting through additive manufacturing. *International Journal of Advanced Manufacturing Technology*. 136(5), 1989-2002. DOI: 10.1007/s00170-024-14979-6.

[2] Chhabra, M. & Singh, R. (2011). Rapid casting solutions: A review. *Rapid Prototyping Journal*. 17(5), 328-350. DOI: 10.1108/13552541111156469.

[3] Kyriakidis, I.F., Kladovasilakis, N., Pechlivani, E.M., & Tsongas, K. (2024). Mechanical performance of recycled 3D printed sustainable polymer-based composites: A literature review. *Journal of Composites Science*. 8(6), 215, 1-28. DOI: 10.3390/jcs8060215.

[4] Deng, C., Kang, J., Shangguan, H., Hu, Y., Huang, T., & Liu, Z. (2018). Effects of hollow structures in sand molds manufactured using 3D printing technology. *Journal of Materials Processing Technology*. 255, 516-523. DOI: 10.1016/j.jmatprotec.2017.12.031.

[5] Zhao, H., Li, L., Ding, S., Liu, C., & Ai, J. (2018). Effect of porous structure and pore size on mechanical strength of 3D-printed combi scaffolds. *Materials Letters*. 223, 21-24. DOI: 10.1016/j.matlet.2018.03.205.

[6] Gunther, D. & Mogele, F. (2016). Additive manufacturing of casting tools using powder binder-jetting technology. *New Trends in 3D Printing*. 53-86. DOI: 10.5772/62532.

[7] Hawaldar, N. & Zhang, J. (2018). A comparative study of fabrication of sand casting mold using additive manufacturing and conventional process. *International Journal of Advanced Manufacturing Technology*. 97(1), 1037-1045. DOI: 10.1007/s00170-018-2020-z.

[8] Sivarupan, T., Balasubramani, N., Saxena, P., Nagarajan, D., El Mansori, M., Salonitis, K., Jolly, M. & Dargusch, M.S. (2021). A review on the progress and challenges of binder jet 3D printing of sand moulds for advanced casting. *Additive Manufacturing*. 40, 101889. DOI: 10.1016/j.addma.2021.101889.

[9] Kosuge, K., Sunaga, M., Goda, R., Onodera, H. & Okane, T. (2018). Cure and collapse mechanism of inorganic mold using spherical artificial sand and water glass binder. *Materials Transactions*. 59(11), 1784-1790. DOI: 10.2320/matertrans.f-m2018838.

[10] Anwar, N., Jalava, K. & Orkas, J. (2023). Experimental study of inorganic foundry sand binders for mold and cast quality. *International Journal of Metalcasting*. 17(3), 1697-1714. DOI: 10.1007/s40962-022-00897-4.

[11] Bobrowski, A. & Grabowska, B. (2012). The impact of temperature on furan resin and binders structure. *Metallurgy and Foundry Engineering*. 38(1), 73-80. DOI: 10.7494/mafe.2012.38.1.73.

[12] Kamińska, J., Puzio, S., Angrecki, M. & Łoś, A. (2020). Effect of reclaim addition on the mechanical and technological properties of moulding sands based on pro-ecological furfuryl resin. *Archives of Metallurgy and Materials*. 65(4), 1425-1429. DOI: 10.24425/amm.2020.133709.

[13] Zheng, J., Hu, X., Tang, B., Qi, T., Pan, Q., Zhu, J., Jia, R., Qui, X., Zhang, Z., Guan, A., Ling, W., Peng, T. & Wang, W. (2024). Promoting sustainability in 3D printed sand casting through adaptive sand mold structures. *Sustainable Materials and Technologies*. 40, e00881, 1-19. DOI: 10.2139/ssrn.4596642.

[14] Sivarupan, T., Balasubramani, N., Saxena, P., Nagarajan, D., El Mansori, M., Salonitis, K., Jolly, M. & Dargusch, M.S. (2021). A review on the progress and challenges of binder jet 3D printing of sand moulds for advanced casting. *Additive Manufacturing*. 40, 101889. DOI: 10.1016/j.addma.2021.101889.

[15] Hegab, H., Khanna, N., Monib, N. & Salem, A. (2023). Design for sustainable additive manufacturing: A review. *Sustainable Materials and Technologies*. 35, e00576, 1-16. DOI: 10.1016/j.susmat.2023.e00576.

[16] Kang, J., Wang, J., Shangguan, H., Zheng, L., Deng, C., Hu, Y. & Yi, J. (2020). Modeling and simulation of the casting process with skeletal sand mold. *Materials*. 13(7), 1596. DOI: 10.3390/ma13071596.

[17] Zheng, L.I., Zhongde, S., Feng, L. & Yuelong, R. (2021). Research of The Influence Mechanism of multi gradient printing on sand mold performance. *Journal of Physics: Conference Series*. 1965(1), 012100. DOI: 10.1088/1742-6596/1965/1/012100.

[18] Hopp, V., Masoudi Alavi, A., Hahn, D. & Quirmbach, P. (2021). Structure–property functions of inorganic chemical binders for refractories. *Materials*. 14(16), 4636, 1-15. DOI: 10.3390/ma14164636.

[19] Wang, F., Cui, X., Yang, Q., Song, H. & Li, D. (2023). Fabrication and posttreatment for inorganic binder jetting sand molds for casting. *Additive Manufacturing*. 73, 103690, 1-15. DOI: 10.1016/j.addma.2023.103690.

[20] Zhang, Z., Jiang, L., Sainoki, A., Peng, X., Li, C., Niu, Q., Wang, X. & Gang, M. (2025). Strengthening effect of particle gradation on the mechanical properties of sand powder 3D printed rock analog. *Journal of Materials Research and Technology*. 35, 1377-1390. DOI: 10.1016/j.jmrt.2025.01.109.

[21] Sivarupan, T., El Mansori, M., Coniglio, N. & Dargusch, M. (2020). Effect of process parameters on flexure strength and gas permeability of 3D printed sand molds. *Journal of Manufacturing Processes*. 54, 420-437. DOI: 10.1016/j.jmapro.2020.02.043.

[22] Xu, J., Kang, J., Hu, Y., Shen, H. & Mao, W. (2024). Study on the mechanical properties of 3D-printed sand mold specimens with complex hollow structures. *Materials*. 17(5), 996, 1-13. DOI: 10.3390/ma17050996.

[23] Gawronová, M., Lichý, P., Kroupová, I., Obzina, T., Beňo, J., Nguyenová, I., Merta, V., Jezierski, J. & Radkovský, F. (2022). Evaluation of additive manufacturing of sand cores in terms of the resulting surface roughness. *Heliyon*. 8(10), e10970. https://doi.org/10.1016/j.heliyon.2022.e10751.

[24] Mocek, J. (2019). Multiparameter assessment of the gas forming tendency of foundry sands with alkyd resins. *Archives of Foundry Engineering*. 19(2), 41-48. DOI: 10.24425/afe.2019.127114.

[25] Liu, L., Shan, Z. & Liu, F. (2018). High-quality manufacturing method of complicated castings based on multi-material hybrid moulding process. *China Foundry*. 15(5), 343-350. DOI: 10.1007/s41230-018-8053-y.

[26] Ye, D. & Zhang, J. (1990). Arbitrary packing of non-equal spherical bodies. *Geological Sciences*. 25(2), 127-136. (in Chinese).

[27] Wang, X., Wu, Q., Huang, Y., Li, N., Wu, X., Chen, X., Wang, J., Jing, T., Huang, T. & Kang, J. (2023). Study on the gas release of 3D-printed furan resin sand core during the casting process. *Materials*. 16(11), 4152, 1-15. DOI: 10.3390/ma16114152.

[28] Mitra, S., de Castro, A.R. & El Mansori, M. (2019). On the rapid manufacturing process of functional 3D printed sand molds. *Journal of Manufacturing Processes*. 42, 202-212. DOI: 10.1016/j.jmapro.2019.04.034.

[29] Wang, Y., Yu, R.L., Yin, S.K., Tan, R. & Lou, Y.C. (2021). Effect of gel time of 3D sand printing binder system on quality of sand mold/core. *China Foundry*. 18(6), 581-586. DOI: 10.1007/s41230-021-1085-8.

[30] Deng, C., Kang, J., Shangguan, H., Hu, Y., Huang, T. & Liu, Z. (2018). Effects of hollow structures in sand molds manufactured using 3D printing technology. *Journal of Materials Processing Technology*. 255, 516-523. DOI: 10.1016/j.jmatprotec.2017.12.031.

[31] Nadimi, S., Mendes, J., López, A., Schröer, L., Manoorkar, S., Ellman, S., Cnudde, V. & Bruno, A. W. (2024). Micro computed tomography images of capillary actions in rough and irregular granular materials. *Scientific Data*. 11(1), 78, 1-7. DOI: 10.1038/s41597-024-02925-w.

[32] Liu, R., Zhao, W., Tian, Y., Zhang, J., Luo, G. & Shen, Q. (2024). Effects of hollow sand mold on the microstructure and mechanical properties of a low-pressure aluminum alloy casting. *Journal of Materials Research and Technology*. 28, 4488-4497. DOI: 10.1016/j.jmrt.2024.01.035.

[33] Haach, V.G., Vasconcelos, G. & Lourenço, P.B. (2011). Influence of aggregates grading and water/cement ratio in workability and hardened properties of mortars. *Construction and Building Materials*. 25(6), 2980-2987. DOI: 10.1016/j.conbuildmat.2010.11.011.

[34] El-Husseiny, A. (2020). Improved packing model for functionally graded sand-fines mixtures—Incorporation of fines cohesive packing behavior. *Applied Sciences*. 10(2), 562, 1-16. DOI: 10.3390/app10020562.